Korean J. Chem. Eng., **24**(3), 466-470 (2007)

Comparison of fractal properties of porous structures during coal devolatilization

Xiaoliang Wang and Rong He†

Department of Thermal Engineering, Tsinghua University, Beijing 100084, China
(*Received 21 August 2006 • accepted 14 November 2006*)

Abstract–This paper investigates fractal property changes of pore structures during coal devolatilization. Similar to char pores, coal pores can also be classified as micro pores and macro pores based on their fractal dimensions. The specific surface area and fractal dimension of micro pores in coal particles are basically unchanged after devolatilization. However, the specific surface area and fractal dimension of macro pores, which are key factors in char combustion, are increased after devolatilization. In fact, the fractal dimensions are basically doubled. These parameters will affect another fractal geometrical factor β in char pores that is correlated to char combustion rate. Since the rate of char combustion can be predicted from their fractal pore properties, it may be possible to predict char combustion directly from the properties of their parent coal pores in the future.

Key words: Fractal, Coal/Char, Pores, Devolatilization

INTRODUCTION

Pore structures of pulverized char particles are very important in char combustion. In pulverized boilers, the pore structures of char particles are formed from their parent coal particles after devolatilization, and the changes of the pore structures during devolatilization affect char combustion rates. The pore structures include specific pore surface area, fractal dimension and other parameters affecting combustion. Therefore, it is necessary to compare some pore properties such as pore specific surface area and fractal dimension before and after devolatilization.

Recently, the changes of pore structures during devolatilization have been measured by means of gas adsorption, X-ray, Scanning Electron Microscopy and mercury porosimetry [1-4]. These researches concern several aspects of pore structures, such as the changes of pore volume distribution [5], total porosity [6], and so on. The pore structures of coal and char particles are fractal-like and the fractal dimensions are also extensively investigated [7-16]. Despite extensive research on pyrolysis, the knowledge on the changes of pore structure is still limited.

There are micro-pores and macro-pores in char pores. Micro pores contribute most of pore surface areas. In general, combustion rate is related to pore surface areas. It is easy to think that large pore surface areas could result in a high combustion rate. However, the large total surface areas do not mean a high reaction rate [17,18]. It has been found recently that char pores can be classified as macro pores and micro pores by a fractal dimension [16,19]. Unlike IUPAC classification of macro-pores (diameter d>50 nm), meso-pores (2<d< 50 nm) and micro-pores (d<2 nm), the classification of macro pores and micro pores by the fractal method reveals effects of fractal properties on char combustion rate through gas diffusion resistance. By defining a fractal geometrical factor β, the char combustion rate can be correlated to macro pore structures [19].

The reference [19] shows how fractal properties of char pores affect char combustion. However, char pores are formed from the parent coal, and we know little of the changes of the fractal properties from coal pores to char pores during devolatilization. This aim of this paper is to investigate the changes of pore structures during coal devolatilization. We compared the fractal properties of different char samples and their parent coal samples. The previous study has shown that the fractal properties of char pores are correlated with char combustion rate. In this paper, how the fractal properties of pores are changed and their meanings to char combustion are discussed.

EXPERIMENTAL

Nine kinds of coal samples were pyrolyzed to produce char samples in a drop-tube furnace filled with nitrogen at 1,200 °C. The drop tube diameter is 50 mm and the flow rate was 8.73 *l*/min. Coal particles were fed at a rate of 1 g/h. The length of drop tube is 1 m and the length of the devolatilization section is 0.8 m and the residual time of coals particles in this section is about 1 seconds. The size of coal particles was about 75 μm. The properties of coal samples are listed Table 1.

Mercury porosimetry is widely used in measuring pore properties for various porous media [9,16,20,21]. In this paper, the pore properties of coal and char were examined by mercury porosimetry. Mercury is forced to penetrate coal and char pores under pressure, and the volume of mercury penetrated V is a function of pressure P. Usually, the Washburn equation can be used to describe the applied pressure P in which mercury enters a pore of radius r:

$$P = -\frac{2\gamma\cos\theta}{r} \tag{1}$$

where γ is the surface tension of mercury (0.48 J/m^2 here) and θ is the mercury-solid contact angle (140° here). The surface area of the pores, S(r), can be calculated by

$$S = \frac{1}{\gamma|\cos\theta|}\int_0^V P\,dV \tag{2}$$

†To whom correspondence should be addressed.
E-mail: rhe@mail.tsinghua.edu.cn
‡This work was presented at the 6th Korea-China Workshop on Clean Energy Technology held at Busan, Korea, July 4-7, 2006.

Table 1. Properties of coal samples

Samples	Proximate analysis (air dry basis)					Ultimate analysis (dry basis)			
	Heating values (cal/g)	Inherent moisture (%)	Ash (%)	Volatile matter (%)	Fixed carbon (%)	C (%)	N (%)	O (%)	S (%)
Shanxi (China)	7,020	2.70	14.5	10.2	72.6	77.9	0.8	2.8	0.4
Yongchen (China)	6,840	1.65	18.4	8.8	71.2	74.7	0.8	2.8	0.4
Datong (China)	6650	7.00	9.70	28.1	55.2	72.3	0.9	11.6	0.8
Hebi (China)	6,980	1.40	16.8	14.2	67.6	74.7	1.3	7.6	0.3
Newlands (Australia)	6,865	3.30	15.9	26.3	57.8	70.7	1.3	7.6	0.3
Chaohua (China)	6,980	1.72	14.	13.0	71.0	77.1	1.2	3.2	0.4
Luoyang (China)	6,890	1.70	16.2	11.5	70.6	75.1	1.3	3.5	0.4
Adaro (Indoesia)	5,950	14.2	1.00	43.8	41.0	72.3	0.8	20.4	0.1
Hongay (Vietnam)	5,950	2.70	25.7	6.10	65.5	67.2	1.1	2.03	0.4

The pressure was increased from the atmosphere pressure to 220 MPa. The minimum radius of pores penetrated by mercury at 220 MPa was about 3.34 nm. The fractal dimension D is defined in the following form

$$\frac{dS(r)}{dr} \propto r^{-D} \tag{3}$$

where S(r) is the accumulated surface area at the corresponding pore radius r. Taking the logarithm on both sides of the above equation, the fractal dimension is the negative value of the slope of ln(dS/dr)~lnr. To analyze the measured data for Eq. (3), the method of 9-moving-points average is used to deal with differential values.

Fractal geometry is widely used in describing highly disordered systems. The geometry of coal/char pores is such a highly disordered system: the pore shape looks irregular. However, many disordered systems, such as coal/char pores, have a characteristic called self-similarity: any part of the system looks like the whole system. This characteristic of self-similarity can be described in scaling power law with a fractal dimension D. There are many ways to define the fractal dimension. The most common definition is called capacity dimension, in which a fractal surface has a fractal dimension between 2 and 3. The fractal dimension in Eq. (3) is defined with the probability density of the pore surface. Usually, the higher the fractal dimension value, the more complex the pore surface. The fractal dimension of char pores can reflect the resistance to gas diffusion in pores [16]. Simply speaking, if a pore surface has high fractal dimension, it means that the geometry of the pore surface is quite complex and it has high resistance to gas diffusion in pores. Therefore, the char combustion rate could be low. However, the char combustion rate is also related to the macro pore surface areas. The effects of the combination of the macro pore surface area and its fractal dimension on char combustion are discussed in [19].

RESULTS AND DISCUSSIONS

Pore structures of both coal samples and char samples are fractal-like, and a typical ln(dS/dr)~lnr plot is illustrated in Fig. 1. Clearly, there are three sections, denoted as I, II and III, that can be fitted as straight lines in Fig. 1. Their slopes are the fractal dimensions defined in Eq. (3) for the three sections, respectively [16,19]. In the experiments, mercury first enters into inter-particle voids, which is represented by Section III. Then, mercury enters macro-pores, which is represented by Section II. With higher pressure mercury can enter micro pores (Section I). The regions of Sections I and Sections II correspond to micro pores and macro pores, respectively, and Section III corresponds to inter-particle voids. Denoting the transit point between Sections I and II as $r_{t,}$, and $r_{t,}$ is the transit radius between macro-pores and micro-pores. Here, unlike IUPAC classification, the definitions of macro pores and micro pores are based only on porous fractal dimensions. Fractal dimension can reflect the complexity of pore geometry, and Eq. (3) shows that small fractal dimension D can lead to highly accumulated pore surface areas. Simply speaking, small D means pore shape is less complex and gas can touch more surface areas. So, in some sense the fractal dimension in Eq. (3) can reflect gas diffusion ability.

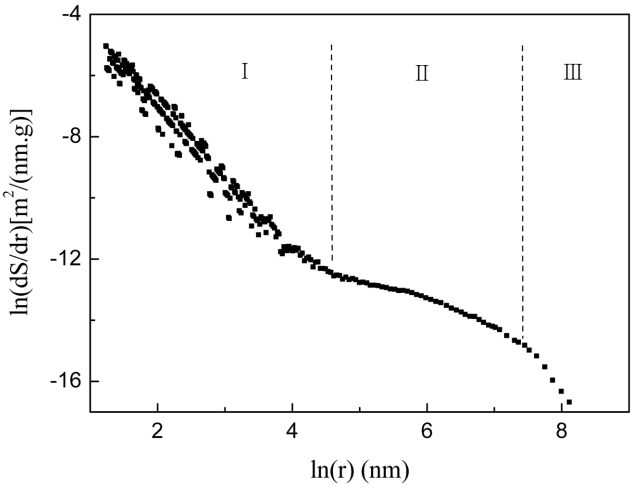

Fig. 1. Three linear sections on ln(dS/dr)~lnr plot (Yongchen coal).

Table 2 lists the fractal dimensions of the coal samples and the values of the transit point $r_{t,}$. For the purpose of comparison, Table 3 lists the fractal dimensions of the char samples.

Comparing Tables 2 and 3, the fractal dimensions of micro pores in char samples are approximately the same as the fractal dimensions of micro pores in coal samples, which means that the pyrolysis does not affect the fractal dimensions of micro pores. However, it can be readily found from these two tables that the fractal dimen-

Table 2. Fractal dimensions of coal samples

Coal sample	D (micro pores)	D (macro pores)	r_{tr} (nm)
Shanxi	2.36±0.02	0.66±0.02	90
Yongchen	2.35±0.03	0.69±0.02	74
Datong	2.39±0.01	0.55±0.01	99
Hebi	2.17±0.03	0.66±0.02	81
Newlands	2.07±0.02	0.70±0.01	129
Chaohua	2.28±0.02	0.75±0.01	73
Luoyang	2.27±0.02	0.74±0.02	81
Adaro	2.73±0.01	0.34±0.02	100
Hongay	2.32±0.02	0.58±0.01	134

Table 3. Fractal dimensions of char samples

Char sample	D (micro pores)	D (macro pores)	r_{tr} (nm)
Shanxi	2.10±0.07	1.20±0.02	76
Yongchen	1.93±0.03	1.32±0.01	49
Datong	1.98±0.03	1.20±0.02	74
Hebi	1.96±0.07	1.16±0.01	53
Newlands	1.95±0.05	0.91±0.02	108
Chaohua	1.92±0.02	1.36±0.01	38
Luoyang	1.84±0.04	1.46±0.02	47
Adaro	2.63±0.02	0.66±0.04	20
Hongay	2.08±0.03	0.78±0.01	105

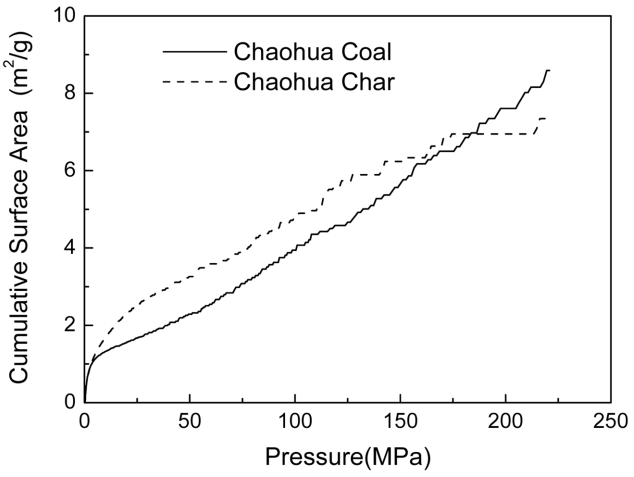

Fig. 2. An illustration of the relation between pressure and cumulative surface areas.

sions of macro pores in most char samples are about twice the fractal dimensions in coal samples. In general, the fractal dimension can be used to describe the complexity of geometrical shapes. The fractal dimension defined in Eq. (3) reflects the gas diffusion ability affected by geometrical structures in some sense. The increase of the fractal dimension of macro pores after devolatilization means that the macro pores of char are more complex than the macro pores of coal, and the resistance of gas diffusion in char macro pores is increased.

Fig. 2 illustrates an example of the relations between pressure and cumulative surface area in mercury porosimetry tests. Total specific surface areas measured by mercury porosimetry usually consist of inter-particle voids S_v, macro-pore S_l and micro-pore S_s. Fig. 3 shows the total specific surface areas of char samples and their parent coal samples. It can be seen that the total specific surface areas are roughly unchanged for most of the samples. But the total specific surface areas are significantly reduced for Shanxi and Hongay samples.

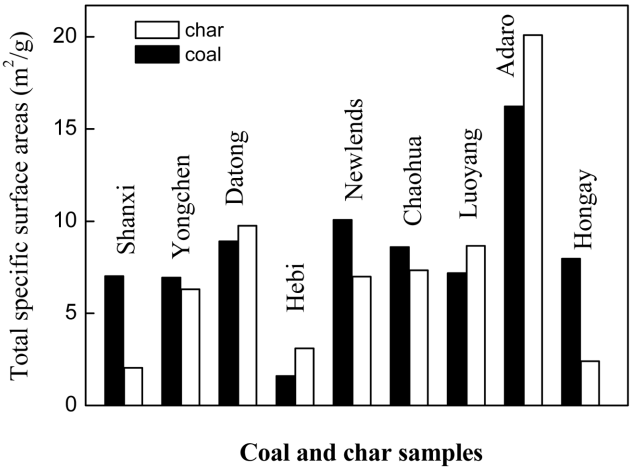

Fig. 3. The total specific surface areas for coal and char samples.

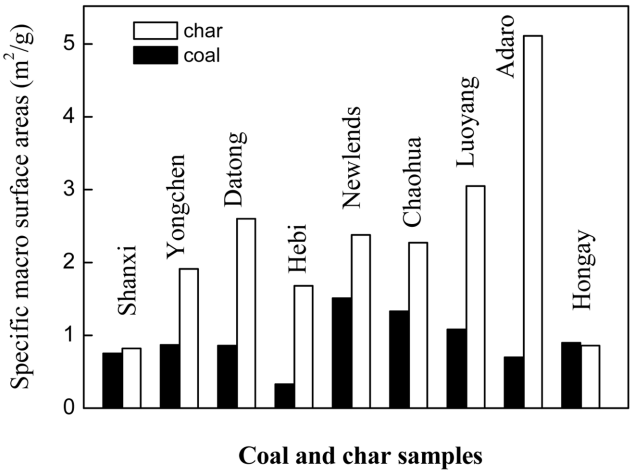

Fig. 4. The specific macro pore surface areas for coal and char samples.

Fig. 4 shows the specific macro pore surface areas of char samples and their parent coal samples. It can be seen that the specific macro pore surface areas of most char samples are significantly increased, and many are doubled. But, for Shanxi and Hongay samples, the specific macro pore surface areas are roughly unchanged before and after devolatilization.

Fig. 5 shows the specific micro pore surface areas of char samples and their parent coal samples. It can be seen that the specific micro pore surface areas of most char samples are slightly reduced or basically unchanged, but some are significantly reduced, especially for Shanxi and Hongay samples.

Although char combustion rate is related to pore surface areas, char combustion occurs mainly in macro pores. The important surface areas are the sum of the specific inter-particle void area and

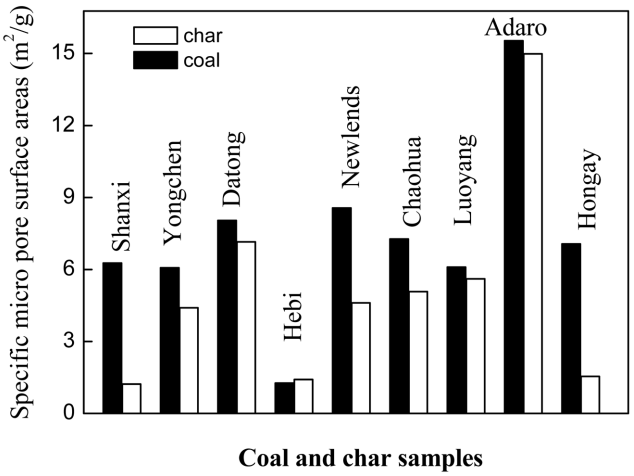

Fig. 5. The specific micro pore surface areas for coal and char samples.

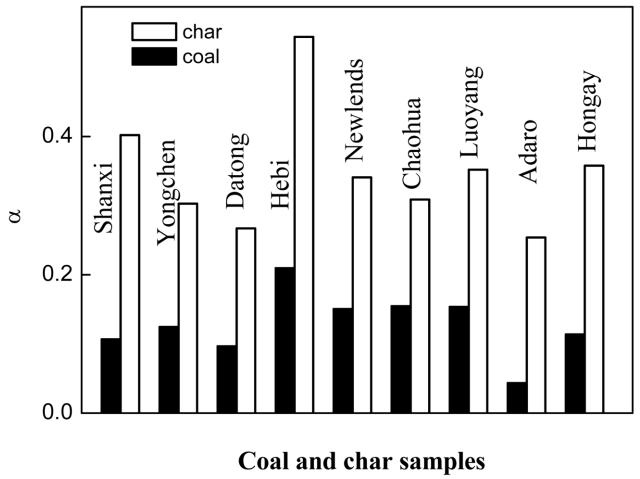

Fig. 6. α values for coal samples and char samples.

the specific macro-pore area S_α ($S_\alpha=S_v+S_l$), which are closely related to char combustion. This can be expressed by the ratio α, which is the ratio of the sum of the specific inter-particle void area and the specific macro-pore area to the total pore surface areas. The α values can reflect the burned fraction of the pore surface areas. As Fig. 6 shows, all the α values are significantly increased after devolatilization. The increasing of the α values is due to the increasing of the specific macro pore surface areas for most samples. But, for the Newlands sample, it is due to both the increase of specific macro pore surface area and decrease of specific micro pore surface area. For Shanxi and Hongay samples, it is due to the significantly reduced specific micro surface areas, although the total specific surface areas are decreased.

In general, a higher α value means a higher ratio of combusted surface areas, hence a higher char combustion rate. However, char combustion within pores is also affected by the fractal dimension of macro pores, which is related to gas diffusion ability within pores. Combining the value of α and the fractal dimension of macro pores, a fractal geometrical factor β is defined in [19] and the char combustion rate is modeled with β. Fig. 6 shows β values are signifi-

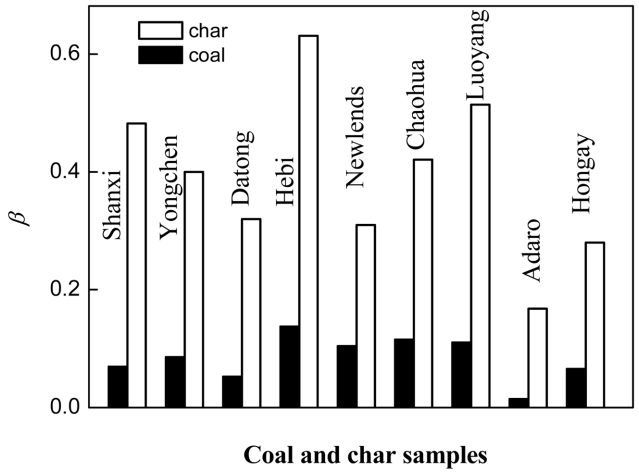

Fig. 7. β values for coal samples and char samples.

cantly increased after devolatilization. Here the β values of coal samples are only for the purpose of comparison, and combustion rates of coal particles may not be described by the β values due to complex pyrolysis and the burn of volatile matters.

The transit radius r_{tr} between macro pores and micro pores, as shown in Tables 2 and 3, is slightly decreased after devolatilization. Usually, for the same coal/char sample, the smaller the transit radius r_{tr} is, the larger the ratio of the macro-pore surface areas to the total pore surface areas is.

The above discussions have depicted a scenario of what happens for pores during high heating rate devolatilization and how it affects char combustion. The total specific pore surface areas of most samples measured by mercury porosimetry are roughly unchanged before and after devolatilization. However, the specific surface areas of macro pores in most samples are increased after devolatilization. Macro pores are important in char combustion and, just from the viewpoint of pore structure, increasing surface areas of macro pores means that char combustion should become easier after devolatilization. However, the fractal dimensions of macro pores are almost doubled after devolatilization, which can increase diffusion resistances within pores and neutralize the effect of increased surface areas of macro pores. The above discussions have roughly shown the combined effects of the changes of surface areas and fractal dimensions on char combustion rates.

CONCLUSIONS

The changes of the pore structures of nine different coals before and after devolatilization are studied. Similar to char pores, coal pores can also be classified as micro-pores and macro-pores based on fractal theory. It is found that the total specific pore surface areas of most samples measured by mercury porosimetry are roughly unchanged before and after devolatilization. However, the specific surface areas of macro pores in most samples are increased after devolatilization, and the ratio of the specific surface areas of macro pores and inter-particle voids to the total specific surface area, i.e., α values in [19], are increased for most samples. Since char combustion mainly occurs in macro pores, these changes after devolatilization will affect char combustion rates significantly. After devolatilization the frac-

tal dimensions are basically doubled for most samples. Previous study has shown that char combustion can be modeled with a fractal geometrical factor β that combines the ratios of the macro-pore surface areas to the total pore surface areas and the fractal dimension of macro pores in char particles. The experimental results in this paper show how the fractal dimensions, the α values and the β values of coal and char particles are changed after devolatilization. In general, increasing surface areas of macro pores makes char combustion faster. But the fractal dimensions of macro pores are almost doubled after devolatilization, which increases diffusion resistances in pores and neutralizes the effect of increased surface areas of macro pores. It may be possible to correlate fractal properties of coal pores directly with char combustion in the future after further study and more understanding of porous structure change during devolatilization.

ACKNOWLEDGMENTS

The authors wish to acknowledge the financial support provided by the China Natural Science Foundations, under Contract No. 50376026.

NOMENCLATURE

D : fractal dimension
P : applied pressure in mercury porosimetry [Pa]
r : pore radius [nm]
r_{tr} : transit radius [nm]
S : total specific reactive surface area [m^2/kg]
S(r) : measured accumulated surface area [m^2/g]
S_l : specific macro-pore area as [m^2/g]
S_s : specific micro-pore area as [m^2/g]
S_t : total specific surface area [m^2/g]
S_v : specific inter-particle void area as [m^2/g]
S_α : sum of the specific inter-particle void area and macro-pore area [m^2/g]

Greek Letters

α : $\alpha = S_\alpha / S_t$
β : geometrical factor; $\beta = \alpha D$
γ : surface tension of mercury [0.48 J/m^2]

REFERENCES

1. C. R. Clarkson and R. M. Bustin, *Fuel*, **78**, 1333 (1999).
2. B. Feng and K. B. Suresh, *Carbon*, **41**, 507 (2003).
3. M. Koichi, A. Hiroyuki, W. C. Xu, G. Rajender, F. W. Terry and T. Akira, *Fuel*, **84**, 63 (2005).
4. B. Ruiz, J. B. Parra, J. A. Pajarea and L. J. Pis, *J. Anal. Appl. Pyrolysis*, **58**, 873 (2001).
5. P. K. Singla, S. Miura, R. R. Hudgins and P. L. Silveston, *Fuel*, **62**, 645 (1983).
6. R. Zajdlik, L. Jelemensky, B. Remiarova and J. Markos, *Chem. Eng. Sci.*, **56**, 1355 (2001).
7. D. Avnir, D. Farin and P. Pfeifer, *J. Colloid Interface Sci.*, **103**, 112 (1985).
8. W. I. Friesen and R. J. Mikula, *J. Colloid Interface Sci.*, **120**, 263 (1987).
9. W. I. Friesen and O. I. Ogunsola, *Fuel*, **74**, 604 (1995).
10. P. J. McMahon, I. K. Snook and W. Treimer, *J. Colloid Interface Sci.*, **252**, 177 (2002).
11. A. C. Mitropoulos, J. M. Haynes, R. M. Richardson, T. A. Steriotis, A. K. Stubos and N. K. Kanellopoulos, *Carbon*, **34**, 775 (1996).
12. T. Nakagawa, K. Nishikawa and I. Komaki, *Carbon*, **37**, 520 (1999).
13. T. Nakagawa, I. Komaki, M. Sakawa and K. Nishikawa, *Fuel*, **79**, 1341 (2000).
14. P. Salatino and F. Zimbardi, *Carbon*, **32**, 51 (1994).
15. S. Hu, M. Li, J. Xiang, L. S. Sun, P. S. Li, S. Su and X. X. Sun, *Fuel*, **83**, 1307 (2004).
16. R. He, X. C. Xu, C. H. Chen, H. Fan and B. Zhang, *Fuel*, **78**, 1291 (1998).
17. P. Ehrburger, F. Louys and J. Lahaye, *Carbon*, **27**, 389 (1989).
18. P. L. J. Walker, *Carbon*, **28**, 261 (1990).
19. R. He, J. Sato and C. H. Chen, *Combust. Sci. Technol.*, **174**, 19 (2002).
20. S. S. Park and H. Y. Kang, *Korean J. Chem. Eng.*, **23**, 367 (2006).
21. K. H. Lee, S. Y. Kim and K. P. Yoo, *Korean J. Chem. Eng.*, **11**, 131 (1994).